Robert Jomar Malate
ES128 Final Project Report

Optimizing Robobee Wing Design using Finite Element Methods

I. Introduction

Robobee wings are complex. In order to find an optimal design, physical experiments need to be conducted. To test just *one* design, a sketch is manually created. It is then fabricated using laminate manufacturing techniques. From there, it is attached to the hinge-and-actuator, placed in front of a high-speed video camera, and the experiments begin. After the experiments, the data is then analyzed by going through the videos manually (refer to ***Figure 1***).

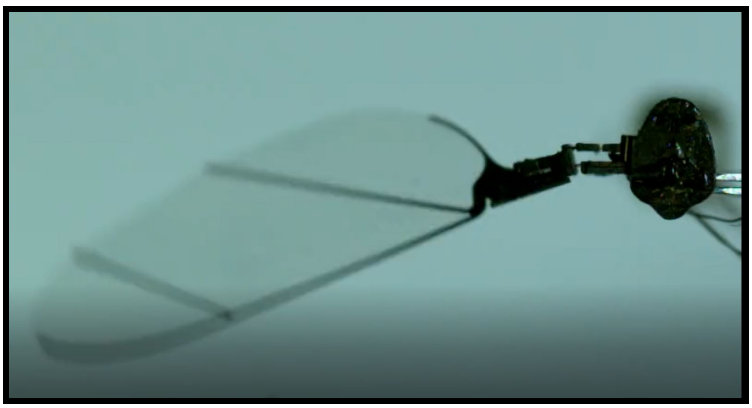

Figure 1: Sample image from a static analysis experiment of the Robobee wing

The whole process takes between 2-3 hours to complete. It is quite tedious and any errors made in the manufacturing process could greatly affect results. This project aims to simplify this process by applying finite element methods via ABAQUS to analyze different wing designs.

II. Goals

For this project, we wanted two things: (1) minimize deflections of the spar and (2) reduce the z-axis moment of inertia. To accomplish this and ensure that the project is within appropriate scope of the class, a couple of parameters were selected. First is (A) spar distance, more specifically, the distance of the right-most spar from a fixed point on the wing, which was the leftmost point of the jigsaw-shaped attachment. Second is (B) spar angle, the angle of both spars relative to the leading edge.

However, due to the many factors involved in the wing design, constraints were also added. We decided to hold the wing area constant, measured to be 54.4 mm^2. The aspect ratio was also kept constant. Refer to ***Figure 2*** for a visual representation of the parameters and

constants. By applying these constraints and selecting these parameters, we can achieve a more optimal wing design that would accomplish our two goals.

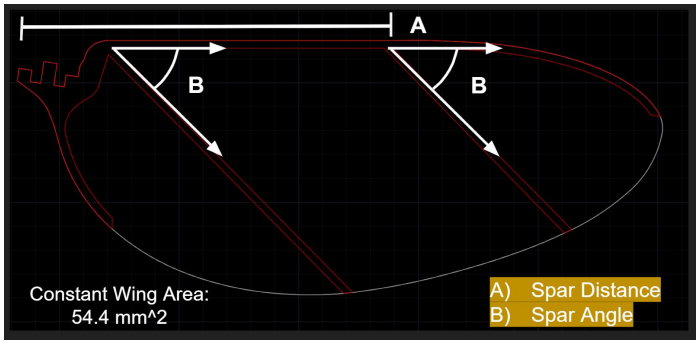

Figure 2: Visual representation of parameters and constraints

---

III. ABAQUS Setup

To ensure that the results we would obtain from the simulations would be as close as we could obtain from physical experimentation, proper setup of the wing model was key. This section describes the process of setting up the model in ABAQUS.

A) Geometry

The foundation to any model is the geometry. Normally, what we would try to do is to recreate the sketches in ABAQUS, and in the Python script, parametrize the geometry.

Unfortunately, this workflow would be challenging to set up due to the complex geometry of the wing. To get around this, an original sketch was modified in AutoCAD, which acted as the reference for all models and the results (note that AutoCAD was primarily used to create the sketches in the beginning). The original sketch geometry was simplified and broken into two parts: the wing frame and the wing membrane (refer to ***Figure 3***). dxf files were then generated from the wing frame sketch and wing membrane sketch. Because of the constraints we applied to the area and aspect ratio, the wing membrane sketch was kept constant, while numerous wing frame sketches were created, each sketch containing a single-modified parameter (refer to ***Figure 4***). By modifying the wing frame shape, we were varying the value of the z-axis moment of inertia, even though we are not directly calculating it. Note that the wing is created in the millimeter scale.

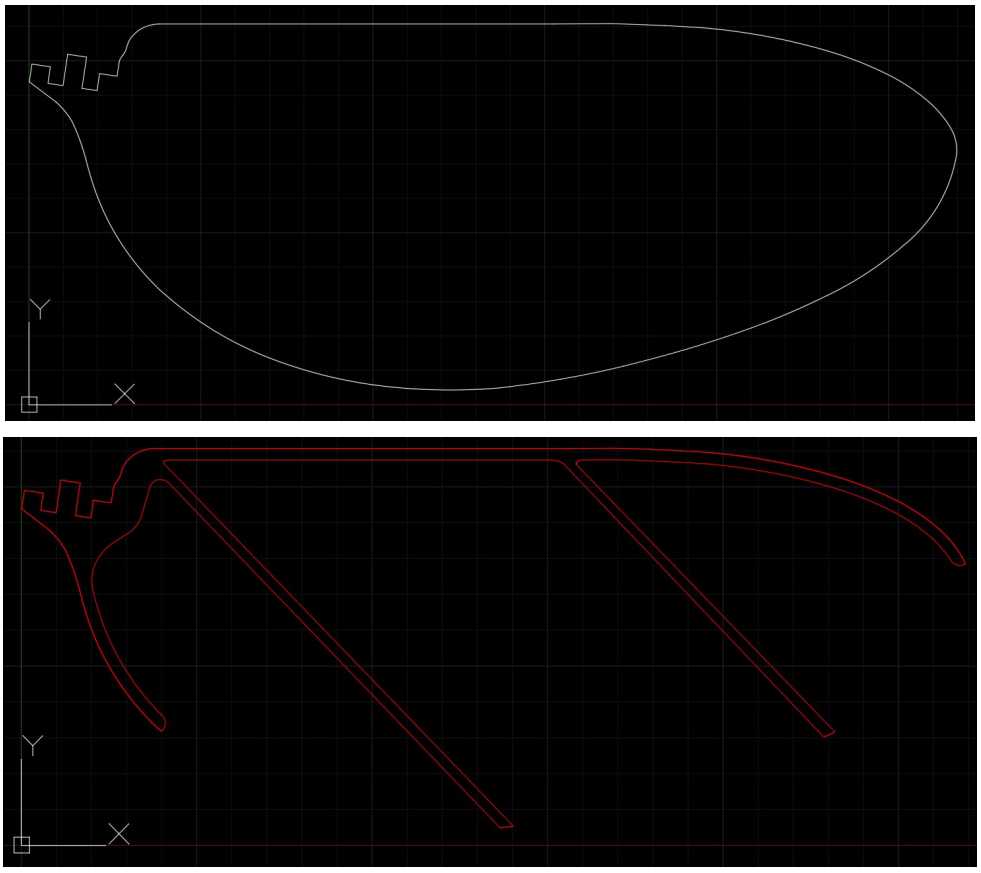

Figure 2: Sketches of wing membrane (top) and wing frame (bottom)

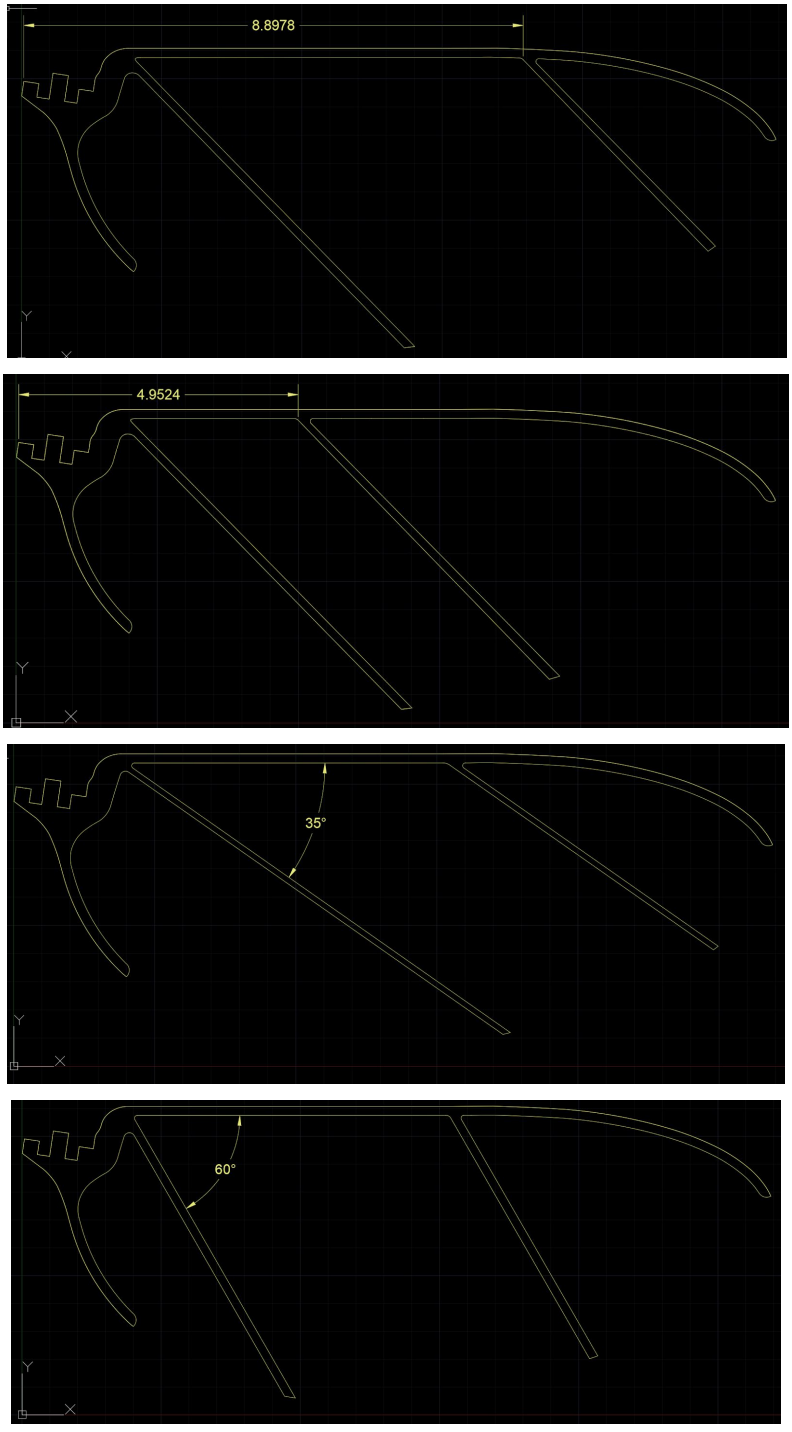

Figure 4: Different wing frame sketches that were created. For the spar length, it ranged between ~5 mm to ~9 mm, measured from the left-most jutting-edge tip of the attachment. For the spar angle, it varied between 35 to 60 degrees.

Each of these dxf files were then imported into ABAQUS, and parts were generated from them. Due to the thin nature of the wings and the shape, each model of the wings was simply the wing membrane with the wing frame sketch partitioned onto it (refer to ***Figure 5***), using 3D shells. This greatly reduced the required computation time.

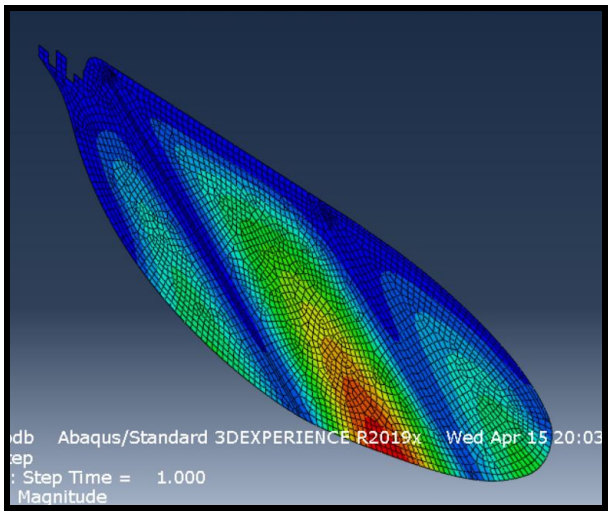

Figure 5: Visualization of 3D shell elements. Notice that the geometry is 2D rather than 3D, which is a feature of using 3D shell elements. Note that the colors don't have any particular meaning for the purposes of this image aside from visualization.

B) Materials

Setting up the materials was much relatively more straightforward than the geometry. The original wing is composed of three layers: the frame, adhesive, and a membrane. Ignoring the adhesive, the materials for the two layers are carbon fiber and Mylar, respectively.

Assuming a linear elastic material, finding the material property values and setting up the Mylar was straightforward [1]. However, setting up the carbon fiber was much more challenging because we wanted to account for the orientations of the fibers. Based on the information given, the orientation of the fibers were 0-45-0 (degrees). Given that the specific brand of carbon fiber was YSH-50, reading the materials sheet for this carbon fiber set, with the help of the class's Teaching Fellow, we were able to extract the relevant material property values [2]. However, the transverse shear modulus G_{23} was not given in the sheet, so we assumed that $G_{13} = G_{23}$. Refer to ***Table 1*** and ***Table 2*** for the values.

Table 1: Mylar material properties	
E (Young's Modulus)	3.447 GPa
ν (Poisson Ratio)	0.38

Table 2: YSH-50 (0-45-0) Carbon fiber material properties	
E_1 (Young's Modulus, 0 deg)	310 GPa
E_2 (Young's Modulus, 90 deg)	3.8 GPa
ν_{12} (In-plane Poisson Ratio)	0.2
G_{12} (In-plane Shear Modulus)	4.8 GPa
G_{13} (Transverse Shear Modulus)	245 GPa
G_{23} (Transverse Shear Modulus)	245 GPa

C) Loading and Boundary Conditions

Crucial to any finite-element analysis is the loads and boundary conditions applied to the structure. Refer to ***Figure 6*** for applied loads and boundary conditions to the model.

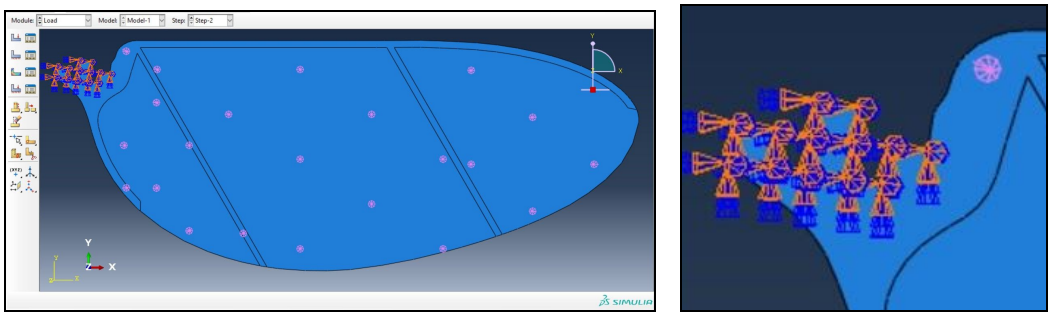

Figure 6: Loads and boundary conditions applied to the model

Because ABAQUS' CFD tool isn't the most reliable and to ensure that the scope of the project was reasonable, we created a static setup, where the aerodynamic drag was changed to a pressure load on the surface of the wing. This is a fair assumption because the drag pressure is always acting perpendicular to the wing surface, and what we care about is the maximum deflection. Since maximum deflection occurs when maximum pressure is applied to the surface, we needed to determine the maximum aerodynamic drag force that was acting on the wing. Using the aerodynamic equations presented in Whitney & Wood's paper [3], we get that $\mathbf{F_{D,max}}$ **=**

6.89 mN, resulting in $\mathbf{P_{max}}$ **= 128 Pa (1.28e-4 MPa)**. Refer to ***Figure 7*** for the equation for calculating F_D.

$$F_L = \tfrac{1}{2}\rho\omega_h^2 C_L(\alpha)\bar{c}R^3 \underbrace{\int_0^1 (\hat{r}+\hat{x}_r)^2\,\hat{c}(\hat{r})\,\mathrm{d}\hat{r}}_{\equiv \hat{F}},$$

Figure 7: Equation to calculate F_D. Note that F_L and C_L are simply switched to F_D and C_D, where C_D is the coefficient of drag. This is listed as Eq. 2.22 in the Whitney & Wood paper.

The boundary conditions were relatively straight-forward. Since the wings were attached to a hinge mechanism that was passively rotating, all translational and rotational degrees of freedom were constrained ($U_1 = U_2 = U_3 = UR_1 = UR_2 = UR_3 = 0$). Although the hinge does allow free rotation, for the static analysis, the hinge is held in place.

D) Meshing

Arguably the most important part of the finite-element method, meshing the wing model was an interesting aspect of the project. Although different mesh elements were tried, ultimately what was used are linear, tetrahedral elements (S3) for the wing frame, and linear, tetrahedral membrane elements (M3D3) for the wing membrane. Refer to ***Figure 8*** for the mesh.

The choice of using linear tetrahedral elements as driven by the failure of the experimental process (Section IV discusses this more extensively). Originally, quad-dominated elements were used, but due to the computational time increase and constant errors being raised, we decided switching over to tetrahedral elements would help us debug the issue. Although quadrilateral elements provide better accuracy, the class's teaching fellows pointed out that linear elements would be satisfactory.

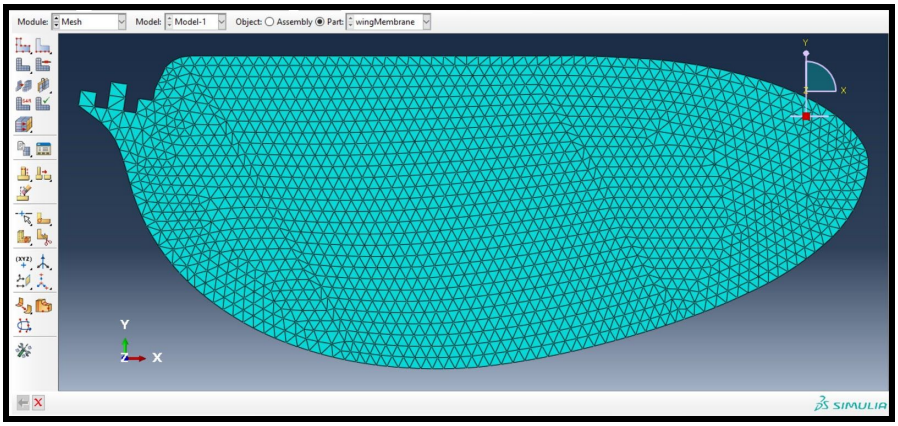

Figure 8: Final Meshing of the Wing

IV. Experimental Process & Results

Despite the numerous methods (that will be discussed in this section) have been tried, due to the complexity and time constraints, we were not able to extract any useful results from the finite element simulations, either because the results were invalid (as in the dynamic explicit simulation) or the jobs did not run at all, which was almost all of the cases. Although no results are provided, this section presents the methods that have been tried, the issues that arose, and potential solutions that were proposed.

A) Method I: Static Analysis

Because we wanted to conduct a static analysis, this was the obvious method to use. Using the setup presented in Section III, we created a static analysis step. Unfortunately, we did not get any useful results. Although the job would run for some time, it crashed eventually, the error being “time increment too small” or “too many attempts made for this increment.” Best case was when the simulation ran up to 20% of the time increments (refer to ***Figure 9***).

Figure 9: Static Analysis test, ran up to ~20% of time increment before aborting due to errors.

To help debug the error, we took a look at the warnings, and what was interesting was the warning “zero MOMENT everywhere” (refer to ***Figure 10***).

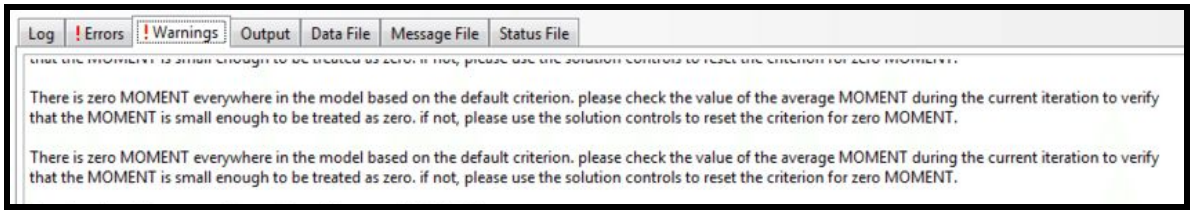

Figure 10: “zero MOMENT everywhere” error.

We concluded that these errors were raised because we were using the bending elements for the Mylar. Membrane elements have no bending stiffness; they behave like fabric

or extremely thin sheets. However, even if we switch the element types to shell elements, we still run into convergence issues.

B) Method II: Dynamic Explicit Analysis

Although using membrane elements led to issues regarding zero moments, a member of the teaching staff pointed out that they've always used membrane elements in dynamic analyses. This led us to our second method: dynamic explicit analysis. Although the dynamic explicit method is prone to inaccuracies, the solution always converges. Additionally, dynamic analyses can be configured to run a quasi-static analysis. Reconfiguring the loading and boundary conditions to run a quasi-static analysis, we were able to get results (refer to ***Figure 11***).

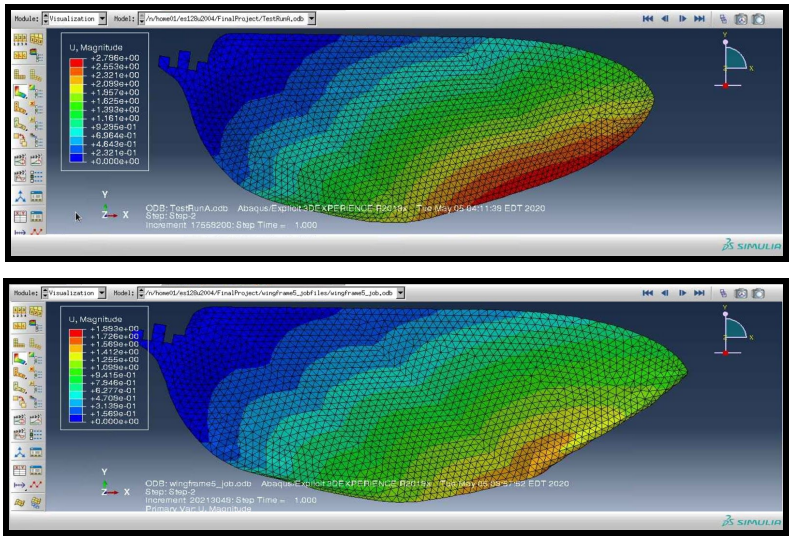

Figure 11: Results of wing analysis from the explicit dynamic analysis.

Unfortunately, these results proved to be unusable due to the oscillations (refer to ***Figure 12***).

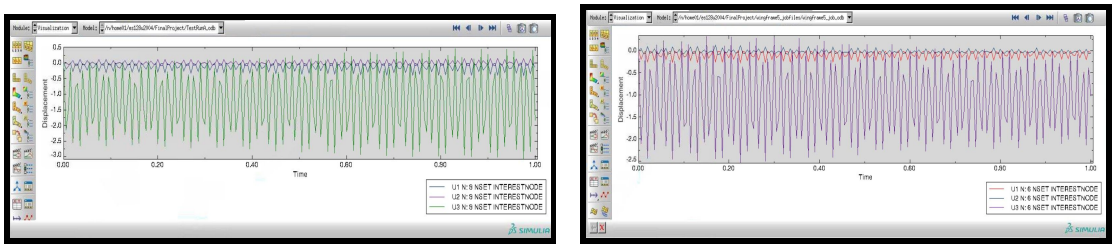

Figure 12: Results of nodal displacement from dynamic explicit analysis. Note the oscillations.

A source of the oscillations comes from mass scaling. In dynamic analysis, mass scaling is done in order to reduce computation time, which in our case was significant, about 4 hours

per wing. However, it does have the effect of creating oscillations in the results. To counteract this, damping is added to the model through changing the bulk damping values in the STEP or material damping. Unfortunately, despite using mass scaling factors ranging from 50 to 1000 while adding a linear bulk viscosity damping factor ranging from 0.06 to 20 and adding material damping of $\alpha = \beta = 0.1$, this balancing act was unable to reduce the computation time and eliminate oscillations.

Another method that we tested out was testing out a smooth step amplitude. Oscillations are created due to accelerations of the model. In order to eliminate this, a smooth step amplitude of the pressure could be applied to the wing (refer to ***Figure 13***). Unfortunately, there was not enough time to test this method out.

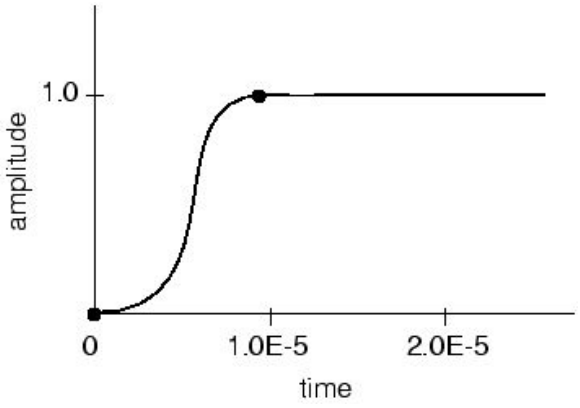

Figure 13: Smooth step function visualization in ABAQUS

C) Method III: Dynamic Implicit Analysis

In an attempt to reduce the errors that occured in the explicit analysis, we switched over to using an implicit, quasi-static analysis. Unfortunately, the analysis did not yield any results at all. The program crashes when I was running the simulation locally, and on the cluster, the time steps were extremely small (Δt = 1.81E-13) that the simulation would not provide results in a reasonable amount of time (refer to ***Figure 14***).

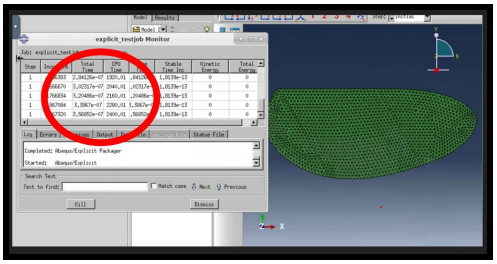

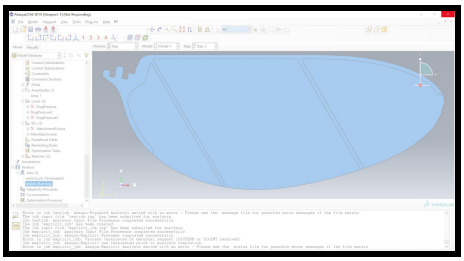

Figure 14: Screenshots of the errors that were encountered when running the implicit analysis.

Material definition was also looked at. For the Mylar, we thought that the errors in convergence could arise due to the potential nonlinear behavior. Using the Lame parameters, we were able to convert the linear elastic parameters to the Neo-Hookean coefficients. ***Table 3*** lists the Neo-Hookean coefficients for Mylar.

Table 3: Mylar hyperelastic material properties	
C10	624.46 MPa
D1	417.76E-06

D) Method IV: Static Analysis using Displacement boundary conditions

The final attempt was to replace the pressure load with a displacement load applied at the rightmost point of the leading edge. Despite this not being the original plan, displacement loads are much more straightforward to compute. Thus, it would help us with the debugging process, and from the results, we could extract the stresses and see which geometry creates the minimum. Unfortunately, this method did not work; convergence issues relating to inadequate time increments were raised. Refer to ***Figure 15*** for a screenshot of the errors.

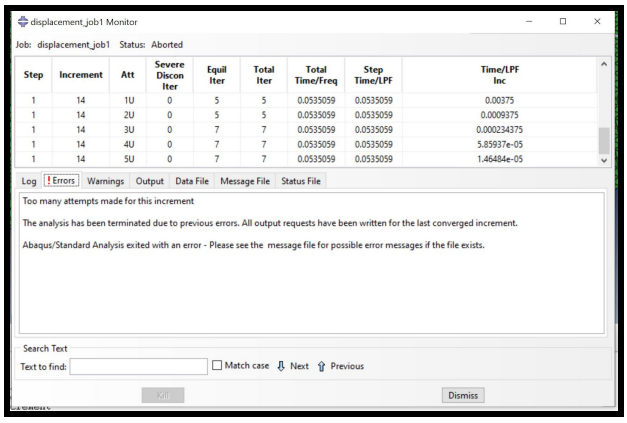

Figure 15: Error raised for Method IV. Error reads "Too many attempts made for this increment."

V. Conclusion and Future Improvements

Although the finite-element analysis (FEA) did not yield any useful results due to technical errors, the process of attempting to model the Robobee wing using FEA via ABAQUS was educational and fruitful. Many new methods and concepts were reinforced and or learned, such as membrane shell elements and the use of dynamic implicit analysis.

However, this doesn't mean that it is impossible not to use FEA to simulate the Robobee wing static experiment. A couple of potential solutions that are worth looking into are the following:

A) ***Adding tensioning to the membrane:*** During manufacturing, the Mylar is stretched out and taut before adding the carbon fiber and adhesive to it. Predefined stress fields could be added just to the membrane, but a method to calculate this needed to be determined.
B) ***Using constraints (ex. tie constraints):*** ABAQUS has a feature that enables surfaces to be bounded together. This would require the two sketches to become two separate parts. This would make it more accurate to the actual wing itself.

In the future, we hope to find a setup that would enable us to simulate the Robobee wings using FEA, using ABAQUS or other available software. Getting good results would enable researchers to compare this to experimental results, and if they are close, could lead to a significant reduction to the time of design of new Robobee wings

VI. Special Thanks & Acknowledgements

I would like to acknowledge several people in this report for their extensive help. I would like to thank Avik De for the inspiration for the project and guidance on retrieving the necessary information to simulate the wing on ABAQUS. Finally, I would like to thank Harvard's ES128/228 teaching staff (Prof. Katia Bertoldi, Connor McCann, Benjamin Gorrisen, and Mohamed Zanaty) for their help and guidance not only throughout the project but also through the entire course of the class.

VII. Citations & Resources

[1] DuPont Teijin Films. (n.d.). *Mylar Polyester Film* (pp. 2–5). Hopewell, VA: DuPont Teijin Films. Retrieved from http://usa.dupontteijinfilms.com/wp-content/uploads/2017/01/Mylar_Physical_Properties.pdf

[2] Yutaka ARAI. (2001). *Pitch-Based Carbon Fiber with Low Modulus and High Heat Conduction* (84th ed., pp. 16–16). Nippon Steel Technical Report. Retrieved from https://www.nipponsteel.com/en/tech/report/nsc/pdf/8403.pdf

[3] Whitney, J., & Wood, R. (2010). Aeromechanics of passive rotation in flapping flight. Journal of Fluid Mechanics, 660, 197-220.